electronics

MDPI

Review

A Review of the Antenna Field Regions

Amedeo Capozzoli [1,*], Claudio Curcio [1], Francesco D'Agostino [2] and Angelo Liseno [1]

[1] Dipartimento di Ingegneria Elettrica e delle Tecnologie dell'Informazione, Università di Napoli Federico II, Via Claudio 21, I-80125 Napoli, Italy; clcurcio@unina.it (C.C.); angelo.liseno@unina.it (A.L.)
[2] Dipartimento di Ingegneria Industriale, Università di Salerno, Via Giovanni Paolo II, 132, I-84084 Fisciano, Italy; fdagostino@unisa.it
* Correspondence: a.capozzoli@unina.it; Tel.: +39-081-7683358

Abstract: We review the field regions and their boundaries around an electromagnetic source. We consider the cases of sources whose dimensions are comparable or larger than the wavelength, of planar sources/apertures, and of sources whose dimensions are small with respect to the wavelength and the criteria involving the strength of the reactive components of the electromagnetic field with respect to the radiative ones. The Fraunhofer and the Fresnel Regions are detailed, along with references to the paraxial approximation for planar apertures. The near-field and intermediate regions are also discussed. We review the standard boundaries between the regions. However, the standard boundaries are not clearly marked, nor are the regions uniquely defined. Accordingly, we also discuss different criteria that have been proposed during the years, which depend on the application and typically rely on numerical arguments, but are not necessarily universally accepted.

Keywords: Fraunhofer region; Fresnel region; near-field region; paraxial region; reactive region; radiative region

1. Introduction

The space around an antenna is typically subdivided into different regions according to the physical behavior of the field and the possible approximations that can be introduced to simplify the field calculation [1–8].

In the standard framework, two different cases are typically considered depending on the dimensions of the source/radiator (antenna): the case of small radiators, when the dimensions are small with respect to the wavelength, and the case of radiators whose dimensions are comparable to or larger than the wavelength. Furthermore, depending on the shape of the source, the cases of linear, planar, or spherical sources can be considered, tailoring the discussion to the case at hand, but keeping the same rationale. Finally, the space around the antenna can be subdivided into two regions according to the strength of the reactive components with respect to the radiative ones.

In the case of antennas whose dimensions are comparable to or larger than the wavelength, it is customary to subdivide the space outside a source according to the hypotheses introduced to simplify the field calculations. The regions are:

The Fraunhofer, or far-field, region;
The Fresnel region;
The near-field region.

In the case of planar sources/apertures whose dimensions are comparable to or larger than the wavelength, the paraxial approximation and a different perspective on field regions can be introduced, leading to the identification of:

The paraxial Fraunhofer region;
The paraxial Fresnel region.

check for updates

Citation: Capozzoli, A.; Curcio, C.; D'Agostino, F.; Liseno, A. A Review of the Antenna Field Regions. *Electronics* **2024**, *13*, 2194. https://doi.org/10.3390/electronics13112194

Academic Editor: David A. Sánchez-Hernández

Received: 6 May 2024
Accepted: 31 May 2024
Published: 4 June 2024

Copyright: © 2024 by the authors. Licensee MDPI, Basel, Switzerland. This article is an open access article distributed under the terms and conditions of the Creative Commons Attribution (CC BY) license (https://creativecommons.org/licenses/by/4.0/).

For a source whose dimensions are small with respect to the wavelength, the Fresnel region is absent, and it is typical to subdivide the space around the radiator into three regions:

The Fraunhofer, or far-field, region;
The intermediate region;
The near-field region.

Finally, when a criterion involving the strength of the reactive components of the field with respect to that of the radiative ones is adopted, the space surrounding the antenna is subdivided into two regions:

Reactive region;
Radiative region.

In the Fraunhofer region of a source, the outgoing wave behaves locally as a plane wave, the field is factorized in its angular and specifical radial dependencies, and the radiation pattern is well defined, being independent of the radial distance. Furthermore, the radial components of the fields are infinitesimal of higher order as compared to the transverse ones as a function of the radial distance. Also, the ratio of the electric and the magnetic far fields should be equal to the intrinsic impedance of the medium. Keeping in mind the conventionality of the definitions of the field boundaries, determining the starting distance of the far field, which can also be regarded as the leading term of the Sommerfeld series [9], is crucial in many applications, since it tells where the radiation pattern starts to be well defined so that antenna performance metrics like gain, sidelobes, beamwidth, and nulls, which are far-field concepts, can be used and estimated from simulations or measurements [10]. In many applications, the transmitter and receiver are located in their reciprocal far-zones so that the field impinging on the receiving antenna is locally plane and the reception can be studied by a canonical wave.

Concerning the Fresnel region, which has been shown to be related to higher-order terms of the Sommerfeld series [9], the related conditions were first derived in [11], while the paraxial Fresnel zone was first numerically analyzed in [12]. The Fresnel zone satisfies similar properties as the Fraunhofer region, except for the fact that any definition of the field pattern would be radially dependent. Efforts have been made throughout the literature to extend concepts and formulas valid for the Fraunhofer region to this zone as well, in view of the need to perform radiation measurements or links in the Fresnel zone [13–16].

The near-field region is the region of space between the radiator and the boundary of the Fresnel region, and the field has a complicated expression therein. Also, for the near-field region, efforts have been made to extend concepts like gain to zones other than the Fraunhofer region [17].

The purpose of this paper is to review the aforementioned field regions [18,19], primarily presenting the standard boundaries between them [20] and providing the technical/mathematical details not reported in [20]. We observe that the definition of the field boundaries is conventional and, thus, not univocal, and the standard boundaries are not clearly marked. Accordingly, we discuss the different criteria that have been proposed during the years, which depend on the application and rely on analytical and/or numerical arguments, and are not necessarily universally accepted across the different application frameworks. The ambiguity in defining the field boundaries can present several drawbacks in practical scenarios:

- Since the behaviors of the radiated field are determined by the distance from the source, ambiguities in defining the field regions can affect antenna placement and design;
- Ambiguities in the field regions can impact the planning and deployment of communication links;
- In medical or industrial applications, when radiation safety is a concern, unclear regions can impair the verification of safety protocols and compliance with exposure regulations;
- Ambiguities in the field regions can result in an unreliable estimate of unintended interference between systems, affecting the overall performance of electronic devices;

- Ambiguities in field regions can impair accurate measurement of electromagnetic fields, especially for antenna characterization, leading to challenges in assessing the performance and compliance of radiators.

To address these challenges, in this paper, we review the definitions of electromagnetic field regions with the aim of facilitating better system design, deployment, and regulatory compliance in various practical applications.

In this paper, the cases of both "volumetric" and of "planar" antennas are considered. For "volumetric" antennas, the field regions are defined by embedding the radiator within a sphere, and their boundaries depend on the diameter of such a sphere. With the antenna enclosed by a symmetrical surface, the boundaries only depend on the distance from the source and not on the observation direction. In the case of "planar" sources, the interest often concerns the definition of the field regions when the radiated field is observed on parallel, planar domains. Under this circumstance, the boundaries between the field regions are defined as long as the observation plane changes, typically along the axis orthogonal to the antenna surface. In this case, approximations, like the paraxial one, are of interest; they hold true around directions close to the axial one and involve the dimensions of both the antenna and the measurement plane.

The paper is organized as follows. In Section 2, the case of antennas whose dimensions are comparable to or larger than the wavelength is dealt with by reviewing the case of sources radiating in the presence of the ground. Furthermore, the case of planar sources/apertures is considered in Section 3. Finally, sources whose dimensions are small with respect to the wavelength, as well as the criteria involving the strength of the reactive components of the field with respect to that of the radiative ones, are addressed in Sections 4 and 5, respectively. In each section, the conditions, the field expressions, the rationale, and the details are outlined. The discussion assumes and drops the $e^{j\omega t}$ time dependence.

2. The Fraunhofer, the Fresnel, and the Near-Field Regions for a Source Contained in a Sphere with Diameter $D > \lambda$

Let us consider a source, as in Figure 1, represented by an electric current density $\underline{J}$ that is occupying a bounded volume V and radiating in the free space. The free space medium is assumed to be homogeneous and lossless, and its dielectric permittivity and magnetic permeability are denoted by real, positive ε and μ, respectively. Addressing the radiating source as an electric one is by no means a limitation, since magnetic current densities can be dealt with in the same way, thanks to duality [18].

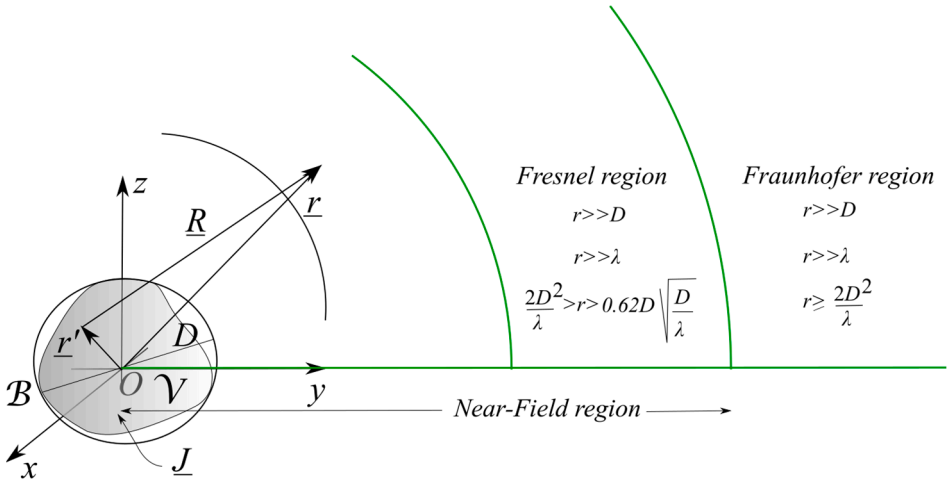

Figure 1. The Fraunhofer, the Fresnel, and the near-field regions for a source contained in a sphere with diameter $D > \lambda$.

We denote with B the smallest sphere enclosing V. The sphere B is assumed to have diameter D and to be centered in a $Oxyz$ Cartesian reference system.

After the standard theory, the vector potential associated with the radiated field is given by [2]:

$$\underline{A}(\underline{r}) = \frac{\mu}{4\pi}\iiint_{\mathrm{V}} \underline{J}(\underline{r}')\frac{e^{-j\beta R}}{R}\mathrm{dV} = \frac{\mu}{4\pi}\frac{e^{-j\beta r}}{r}\iiint_{\mathrm{V}} \frac{r}{R}\underline{J}(\underline{r}')e^{-j\beta(R-r)}\mathrm{dV}, \tag{1}$$

where $\underline{r}$ represents the point at which the field is observed, $\underline{r}'$ is the vector position of the generic source point, $\beta = \omega\sqrt{\varepsilon\mu}$ is the wavenumber, λ is the wavelength, and $\underline{R} = \underline{r} - \underline{r}'$. In Equation (1), $r = |\underline{r}|$ and $R = |\underline{R}|$.

The electric field $\underline{E}$ and the magnetic field $\underline{H}$ outside the source region V can be calculated from Equation (1) as [2]:

$$\underline{E}(\underline{r}) = \frac{1}{4\pi j\omega\varepsilon}\iiint_{\mathrm{V}} \left[\beta^2\underline{J}(\underline{r}')\frac{e^{-j\beta R}}{R} + (\underline{J}(\underline{r}')\cdot\nabla)\nabla\left(\frac{e^{-j\beta R}}{R}\right)\right]d\mathrm{V}, \tag{2}$$

$$\underline{H}(\underline{r}) = \frac{1}{4\pi}\iiint_{\mathrm{V}} \nabla\left(\frac{e^{-j\beta R}}{R}\right)\times\underline{J}(\underline{r}')\mathrm{dV}. \tag{3}$$

After straightforward manipulations, Equations (2) and (3) can be rewritten as [5]:

$$\underline{E}(\underline{r}) = \frac{-j\beta\zeta}{4\pi}\frac{e^{-j\beta r}}{r}\iiint_{\mathrm{V}} \frac{r}{R}\left[(\underline{\underline{I}} - \hat{R}\hat{R}) + (\underline{\underline{I}} - 3\hat{R}\hat{R})\left(\frac{1}{j\beta R} + \frac{1}{(j\beta R)^2}\right)\right]\underline{J}(\underline{r}')e^{-j\beta(R-r)}d\mathrm{V}, \tag{4}$$

$$\underline{H}(\underline{r}) = \frac{1}{4\pi}\frac{e^{-j\beta r}}{r}\iiint_{\mathrm{V}} \frac{r}{R}\left(1 + \frac{1}{j\beta R}\right)(-j\beta\hat{R})\times\underline{J}(\underline{r}')e^{-j\beta(R-r)}d\mathrm{V}, \tag{5}$$

where $\underline{\underline{I}}$ is the identity dyadic tensor and $\zeta = \sqrt{\frac{\mu}{\varepsilon}}$ is the intrinsic impedance of the medium.

The behavior at infinity of the quantities $\frac{1}{R}$, $\hat{R}$, and $\frac{R-r}{r}$ appearing in Equations (1), (4), and (5) is given by:

$$\frac{1}{R} = \frac{1}{r} + o_{+\infty}\left(\frac{1}{r}\right), \tag{6}$$

$$\hat{R} = \hat{r} + o_{+\infty}(1), \tag{7}$$

$$\frac{R-r}{r} = -\frac{r'}{r}(\hat{r}\cdot\hat{r}\prime) + \frac{1}{2}\left(\frac{r'}{r}\right)^2\left(1 - (\hat{r}\cdot\hat{r}\prime)^2\right) + \frac{1}{2}\left(\frac{r'}{r}\right)^3(\hat{r}\cdot\hat{r}\prime)\left(1 - (\hat{r}\cdot\hat{r}\prime)^2\right) + o_{+\infty}\left(\left(\frac{r'}{r}\right)^3\right), \tag{8}$$

$o_{+\infty}(\cdot)$ being the little-o Bechmann–Landau symbol, defined in [21], which identifies, in Equations (6)–(8), infinitesimals whose order is higher than that of the argument. Equations (6)–(8) will be exploited shortly to define the field regions for sources contained in a sphere with diameter $D > \lambda$.

2.1. The Fraunhofer Region or Far-Field Region

The Fraunhofer region or far-field region is that portion of space wherein the fields can be calculated following the assumptions:

$$r \gg D; \tag{9a}$$

$$r \gg \lambda; \tag{9b}$$

$$r > \frac{2D^2}{\lambda}. \tag{9c}$$

The above assumptions define the exterior of a sphere centered at the origin O of the $Oxyz$ reference system in Figure 1.

The first two conditions (9a) and (9b) allow the approximation of the "amplitude terms" in Equations (1), (4), and (5) as:

$$\frac{r}{R} \cong 1, \tag{10}$$

$$\frac{r}{R}\left(1+\frac{1}{j\beta R}\right)\hat{R} \cong \hat{r}, \tag{11}$$

$$\frac{r}{R}\left[\left(\underline{\underline{I}}-\hat{R}\hat{R}\right)+\left(\underline{\underline{I}}-3\hat{R}\hat{R}\right)\left(\frac{1}{j\beta R}+\frac{1}{(j\beta R)^2}\right)\right] \cong \left(\underline{\underline{I}}-\hat{r}\hat{r}\right). \tag{12}$$

It should be noticed that, when applied to a generic vector $\underline{V}$, the operator $\left(\underline{\underline{I}}-\hat{r}\hat{r}\right)$ returns $\hat{r}\times(\underline{V}\times\hat{r})$.

Concerning the exponential term in Equations (1), (4), and (5), and after neglecting contributions of order higher than the first in $\frac{r'}{r}$ in Equation (8), condition (9c) allows the following approximation:

$$e^{-j\beta(R-r)} \cong e^{j\beta r'(\hat{r}\cdot\hat{r}')}. \tag{13}$$

In particular, the first term neglected in Equation (8) is the quadratic one in $\frac{r'}{r}$. Assuming that such a quadratic term is the most relevant one among the remaining neglected ones, it is supposed that:

$$e^{-j\beta r\left[\frac{r'^2}{2r^2}\left(1-(\hat{r}\cdot\hat{r}')^2\right)\right]} \cong 1. \tag{14}$$

The standard criterion to accept Equation (14) assumes:

$$\beta\frac{(D/2)^2}{2r} < \frac{\pi}{8} \leftrightarrow r > \frac{2D^2}{\lambda}. \tag{15}$$

In Equation (15), to consider the worst case, the maximum value for r' is set equal to $D/2$. Some authors request a lower phase error, say, $\pi/(\xi 8)$, with $\xi > 1$, for accurate measurements of low sidelobes so that condition (15) becomes $r > 2\xi D^2/\lambda$ [22].

After Equations (10)–(13), the field expressions in Equations (1), (4), and (5) turn into the following:

$$\underline{A}_\infty(\underline{r}) = \frac{\mu}{4\pi}\frac{e^{-j\beta r}}{r}\iiint_V \underline{J}(\underline{r}')e^{j\beta r'(\hat{r}\cdot\hat{r}')}\mathrm{dV}, \tag{16}$$

$$\underline{H}_\infty(\underline{r}) = \frac{1}{\mu}(-j\beta\hat{r})\times\underline{A}_\infty(\underline{r}), \tag{17}$$

and

$$\underline{E}_\infty(\underline{r}) = \zeta\underline{H}_\infty(\underline{r})\times\hat{r} = \frac{e^{-j\beta r}}{r}\underline{F}_\infty(\hat{r}), \tag{18}$$

where $\underline{F}_\infty$ is the Fraunhofer pattern or the far-field pattern. As can be seen from Equation (18), the Fraunhofer pattern depends only on the observation direction $\hat{r}$ so that the concept of the far-field radiation pattern is well defined and applies.

From Equations (17) and (18), the fields in the Fraunhofer region have the following properties:

- $\underline{E}_\infty\cdot\hat{r} = 0$;
- $\underline{H}_\infty\cdot\hat{r} = 0$;
- $\underline{H}_\infty = \frac{1}{\zeta}\hat{r}\times\underline{E}_\infty$;
- $\underline{S}_\infty = \frac{1}{2\zeta}|\underline{E}_\infty|^2\hat{r} = \frac{\zeta}{2}|\underline{H}_\infty|^2\hat{r}$.

In particular, the fields have local plane wave behavior with the propagation direction defined by $\hat{r}$, with $\underline{E}$ and $\underline{H}$ being orthogonal to the observation direction $\hat{r}$, mutually

orthogonal, and satisfying the "impedance relation" $\frac{|\underline{E}_\infty|}{|\underline{H}_\infty|} = \zeta$ [23]. Furthermore, the Poynting vector is real and radially oriented [23]. In this region, knowing the $\underline{E}$ field enables the knowledge of the $\underline{H}$ field or vice versa, as well as the knowledge of the Poynting vector.

Conditions (9a)–(9c) above fix the universally accepted far-field conditions. However, how they should be interpreted from a practical point of view, as well as the difficulties of defining a sharp far-field boundary, have been the subject of much discussion throughout the literature [6,24–26]. Different authors have proposed different, mainly numerical, criteria. Hence, we point out the most popular ones. Nevertheless, they should not be used as replacements for the standard theory, but just as points of discussion.

In particular, recently, conditions (9a)–(9c) were analyzed simultaneously for dipole antennas of lengths $\frac{\lambda}{2}$ and λ in [27]. Requiring that the reactive field terms in the Fraunhofer region be negligible as compared to the radiative one and that the radial components of the fields be negligible as compared to the transverse ones, far-field boundaries at distances of 9.5λ and 12λ for the half-wave and full-wave dipole, respectively, were calculated.

Furthermore, for dipoles of more general lengths, Ref. [26] proposed the following re-statements of conditions (9a)–(9c):

$$r \geq 5D; r \geq 1.6\lambda. \tag{19}$$

Concerning (9a)–(9c), it has been also underlined that they are sometimes misused by practitioners that employ the only (9c) condition to define the starting boundary of the far-field region. This point was outlined in [26], where some analytical arguments are also presented to claim that (9c) alone can be considered as the far-field boundary only if $D \geq 5\lambda$. A less restrictive condition, $D \geq 2.5\lambda$, was derived in [28] using numerical arguments. Still, numerically, and again in [28], it has been pointed out how, for sources having $\frac{\lambda}{3} < D < 2.5\lambda$, the far-field boundary can be set at $r \geq 5D$.

As already mentioned in the Introduction, the far field is crucial in many applications since it enables the definition of antenna performance metrics like gain, sidelobes, beamwidth, and nulls, which are far-field concepts. Furthermore, the radiation pattern of an antenna in the far-field zone does not change with distance, and so it is "stable" and "predictable", enabling most of the antenna links to be far-field ones. Finally, the definition of the far field and of the local plane wave behavior of the field radiated by a source is crucial in the typical modeling of the reception process of sensing probes, as underlined in the Appendix A.

2.2. The Fresnel Region

The Fresnel region [9,12] is that portion of space wherein the fields can be calculated following the assumptions:

$$r \gg D; \tag{20a}$$

$$r \gg \lambda; \tag{20b}$$

$$\frac{2D^2}{\lambda} > r > 0.62D\sqrt{\frac{D}{\lambda}} \tag{20c}$$

The above assumptions define a spherical shell centered at the origin O of the $Oxyz$ reference system in Figure 1.

The first two conditions, (20a) and (20b), allow the same approximations expressed by Equations (10)–(12) in Equations (1), (4), and (5). On the other side, condition (20c) leads to an approximation of the exponential term $e^{-j\beta(R-r)}$ which is different from that in Equation (14). Indeed, after neglecting contributions of higher order than the second in $\frac{r'}{r}$ in Equation (8), condition (20c) allows the following approximation:

$$e^{-j\beta(R-r)} \cong e^{j\beta r'(\hat{r}\cdot\hat{r}')} e^{-j\beta[\frac{r'^2}{2r^2}(1-(\hat{r}\cdot\hat{r}')^2)]}. \tag{21}$$

In particular, the first term neglected in Equation (8) is now the cubic one in $\frac{r'}{r}$. Assuming such a cubic term to be the most relevant among the neglected remaining ones, it is now supposed that:

$$e^{-j\beta r\left[\frac{1}{2}\left(\frac{r'}{r}\right)^3(\hat{r}\cdot\hat{r}')(1-(\hat{r}\cdot\hat{r}')^2)\right]} \cong 1. \tag{22}$$

The standard criterion to accept Equation (22) assumes:

$$\beta\frac{(D/2)^3}{2r^2}\frac{\sqrt{3}}{3}\frac{2}{3} < \frac{\pi}{8} \leftrightarrow r > 0.62\mathrm{D}\sqrt{\frac{D}{\lambda}}. \tag{23}$$

where, as before, to consider the worst case, the maximum value for r' is set equal to $D/2$.

After Equations (10)–(12) and (21), the field expressions in Equations (1), (4), and (5) turn into the following:

$$\underline{A}_F(\underline{r}) = \frac{\mu}{4\pi}\frac{e^{-j\beta r}}{r}\iiint_V \underline{J}(\underline{r}')e^{j\beta r'(\hat{r}\cdot\hat{r}')}e^{-j\beta\left[\frac{r'^2}{2r^2}(1-(\hat{r}\cdot\hat{r}')^2)\right]}\mathrm{dV}, \tag{24}$$

$$\underline{H}_F(\underline{r}) = \frac{1}{\mu}(-j\beta\hat{r}) \times \underline{A}_F(\underline{r}), \tag{25}$$

and

$$\underline{E}_F(\underline{r}) = \zeta\underline{H}_F(\underline{r}) \times \hat{r} = \frac{e^{-j\beta r}}{r}\underline{F}_F(r,\hat{r}), \tag{26}$$

where $\underline{F}_F$ is the Fresnel pattern. As can be seen from Equation (26), the Fresnel pattern, unlike the Fraunhofer pattern, depends on both the observation direction $\hat{r}$ and the radial distance r.

As for the Fraunhofer region, the fields in the Fresnel region satisfy the following conditions, as stated by Equations (25) and (26):

- $\underline{E}_F \cdot \hat{r} = 0$;
- $\underline{H}_F \cdot \hat{r} = 0$;
- $\underline{H}_F = \frac{1}{\zeta}\hat{r} \times \underline{E}_F$;
- $\underline{S}_F = \frac{1}{2\zeta}|\underline{E}_F|^2\hat{r} = \frac{\zeta}{2}|\underline{H}_F|^2\hat{r}$.

In particular, the fields have local plane wave behavior with the propagation direction defined by $\hat{r}$, with $\underline{E}$ and $\underline{H}$ orthogonal to the observation direction $\hat{r}$, mutually orthogonal, and satisfying the "impedance relation" $\frac{|E_\infty|}{|H_\infty|} = \zeta$ [23]. Furthermore, the Poynting vector is, again, real and radially oriented [23]. In this region, knowing the $\underline{E}$ field enables the knowledge of the $\underline{H}$ field or vice versa, as well as, in addition, the knowledge of the Poynting vector. However, differently from the far-field region, the angular field distribution is distance-dependent, and the concept of a radiation pattern meant as an entity depending only on angular spherical coordinates is not applicable.

Finally, it should be noted that condition (20c), defining the Fresnel region, can be rewritten as:

$$\sqrt{\frac{D}{\lambda}} > \frac{r}{2D\sqrt{\frac{D}{\lambda}}} > 0.31. \tag{27}$$

Accordingly, as long as the source dimension D becomes smaller than the wavelength, the Fresnel region disappears.

In microwave applications, such as antenna measurements, radar systems, or inverse problems in general, understanding the Fresnel zone becomes particularly important. Indeed, regarding radar systems, including synthetic aperture radar (SAR), target imaging is performed when the data are collected in the Fresnel zone of the objects [29]. Furthermore, antenna characterization approaches using Fresnel-zone-to-far-field transformations have been also proposed [30]. Finally, in direct and inverse problems, analyzing the unknowns-

to-data links for measurements in the Fresnel zone helps in deriving estimations of radiated fields and analytical forecasts of the performance of inversion approaches [31–34].

2.3. The Near-Field Region

The near-field region [23,25,35] is the region of space surrounding the source that satisfies the condition:

$$FB > r > \frac{D}{2}, \tag{28}$$

where FB defines the Fresnel boundary.

These inequalities define a spherical shell centered at the origin O of the $Oxyz$ reference system in Figure 1. In other words, the near-field region is a spherical shell included between the source and the boundary of the Fresnel region. Therein, no general approximations are typically introduced to simplify the field calculation. In particular, the radiating pattern is distance-dependent:

Understanding and characterizing the near-field region is crucial in various scenarios for optimizing performance, ensuring reliable communication, and enhancing the overall functionality of the systems involved, as, for example, in:

- Wireless communications of the future, e.g., 6G, to study the potential benefits and new design challenges which arise from near-field connections for optimizing signal strength and minimizing interference [36,37];
- Radio-frequency identification (RFID) and near-field communication (NFC) systems, for which understanding the structure of the near field plays a key role in designing an effective communication system between the RFID reader and the tag or for secure data exchange between devices [38,39];
- Medical imaging, like microwave imaging or magnetic resonance imaging (MRI), for which knowledge of the near field is crucial for accurate reconstruction [40];
- Near-field measurements for the amplitude and phase or phaseless characterization of antennas [41,42].

3. The Fraunhofer and the Fresnel Regions for a Planar Source with Dimension Comparable to or Larger Than the Wavelength λ: Standard and Paraxial Approximations

The Fraunhofer and the Fresnel regions for planar apertures can be dealt with in a way that is analogous to that in Section 2 [25]. Here, the formulation considers a planar aperture, but the case of planar current densities can be dealt with in a totally similar way. In addition, for this case, the alternative paraxial approximation can be introduced [4,6], and some details about it can also be rephrased.

Figure 2 shows the relevant geometry for the present case, which involves a planar radiating aperture A. A Cartesian $Oxyz$ reference system is considered with the origin O at the center of A, so that the radiating aperture lies in the $z = 0$ plane. The smallest square containing the aperture is assumed to have linear length D. Finally, the half-space $z > 0$ is assumed to be source-free and the embedding medium to be homogeneous and lossless, as in the previous section.

Following [5], the fields in the half-space $z > 0$ can be written as:

$$\underline{E}(\underline{r}) = \frac{-j\beta}{2\pi}\frac{e^{-j\beta r}}{r}\iint_{\mathrm{A}}\frac{r}{R}\left(1+\frac{1}{j\beta R}\right)e^{-j\beta(R-r)}\hat{R}\times\left(\hat{z}\times\underline{E}(\underline{r}')\right)dx'dy', \tag{29}$$

$$\underline{H}(\underline{r}) = \frac{j\beta}{2\pi\zeta}\frac{e^{-j\beta r}}{r}\iint_{\mathrm{A}}\frac{r}{R}\left[\left(\underline{\underline{I}}-\hat{R}\hat{R}\right)+\left(\underline{\underline{I}}-3\hat{R}\hat{R}\right)\left(\frac{1}{j\beta R}+\frac{1}{(j\beta R)^2}\right)\right]e^{-j\beta(R-r)}\left(\hat{z}\times\underline{E}(\underline{r}')\right)dx'dy'. \tag{30}$$

with the same meaning as the symbols in Section 2.

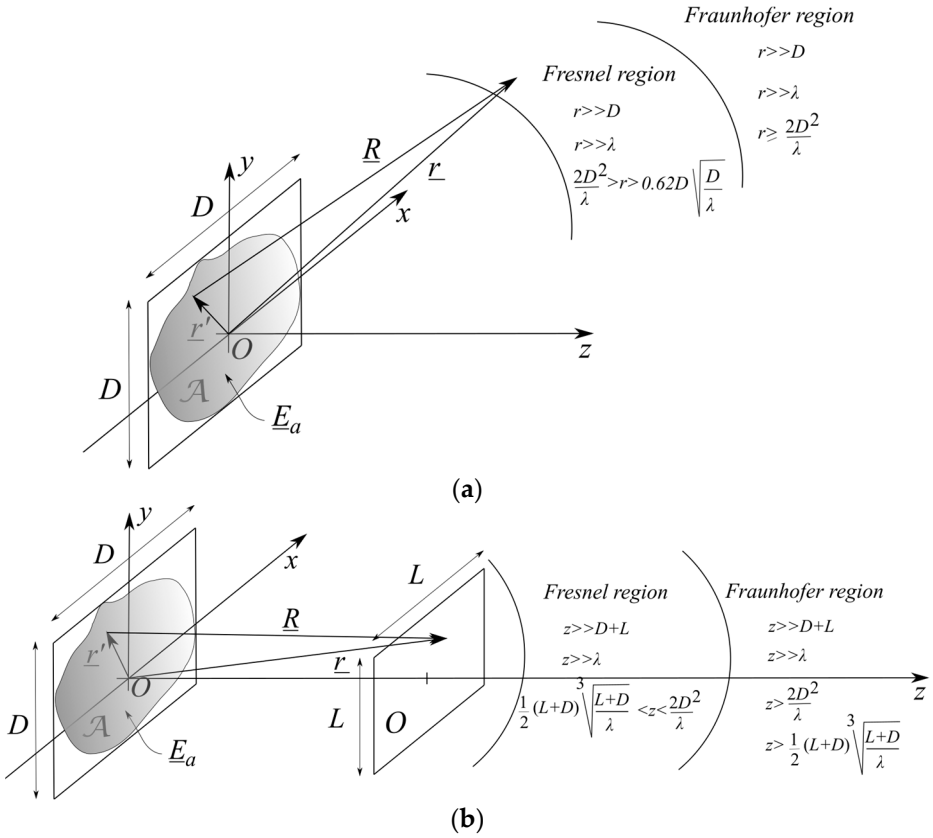

Figure 2. The Fraunhofer and the Fresnel regions for a planar source with dimensions comparable to or larger than λ: (**a**) standard and (**b**) paraxial approximations.

When the fields are evaluated in the proximity of the z-axis, the paraxial approximation can be introduced [43,44]. In more detail, the fields are assumed to be observed on a square O orthogonal to and centered around the z-axis, set a distance $z > 0$ apart from the aperture plane $z = 0$ and with maximum linear dimension L. The simplifying hypothesis essentially assumes that the (transverse) dimensions of both the aperture A and the observation domain O are small with respect to their reciprocal distance z.

To clarify the role of the conditions and to obtain the approximated field expressions under the paraxial approximation, it is convenient to rewrite Equations (29) and (30) as:

$$\underline{E}(\underline{r}) = \frac{-j\beta}{2\pi}\frac{e^{-j\beta z}}{z}\iint_{\mathrm{A}}\frac{z}{R}\left(1+\frac{1}{j\beta R}\right)e^{-j\beta(R-z)}\hat{R}\times\left(\hat{z}\times\underline{E}\left(\underline{r}'\right)\right)dx'dy', \tag{31}$$

$$\underline{H}(\underline{r}) = \frac{j\beta}{2\pi\zeta}\frac{e^{-j\beta z}}{z}\iint_{\mathrm{A}}\frac{z}{R}\left[\left(\underline{I}-\hat{R}\hat{R}\right)+\left(\underline{I}-3\hat{R}\hat{R}\right)\left(\frac{1}{j\beta R}+\frac{1}{(j\beta R)^2}\right)\right]e^{-j\beta(R-z)}\left(\hat{z}\times\underline{E}\left(\underline{r}'\right)\right)dx'dy'. \tag{32}$$

3.1. The Fraunhofer or Far-Field Region for a Planar Aperture

Following Section 2.1, the conditions defining the Fraunhofer or far-field region are:

$$r \gg D; \tag{33a}$$

$$r \gg \lambda; \tag{33b}$$

$$r > \frac{2D^2}{\lambda}. \tag{33c}$$

The related field expressions can be obtained straightforwardly after some manipulations of Equations (29) and (30). In particular:

$$\underline{E}_{\infty}(\underline{r}) = \frac{1}{2\pi}\frac{e^{-j\beta r}}{r}(-j\beta\hat{r}) \times \iint\limits_{A} e^{j\beta r'(\hat{r}\cdot\hat{r}')}\left(\hat{z} \times \underline{E}(\underline{r}')\right)dx'dy\prime, \tag{34}$$

$$\underline{H}_{\infty} = \frac{1}{\zeta}\hat{r} \times \underline{E}_{\infty} \tag{35}$$

Analogous discussion and the properties as in Section 2.1 also apply now. The results of Equations (32) and (33) are of interest in a large number of applications involving optics and radio/microwave propagation. For an analytical derivation, see [44].

3.2. The Fresnel Region for a Planar Aperture

Following Section 2.2, the conditions defining the Fresnel region are [44]:

$$r \gg D; \tag{36}$$

$$r \gg \lambda; \tag{37}$$

$$\frac{2D^2}{\lambda} > r > 0.62D\sqrt{\frac{D}{\lambda}}. \tag{38}$$

The related field expressions can be obtained straightforwardly after some manipulations of Equations (29) and (30):

$$\underline{E}_F(\underline{r}) = \frac{1}{2\pi}\frac{e^{-j\beta r}}{r}(-j\beta\hat{r}) \times \iint\limits_{A} e^{j\beta r'(\hat{r}\cdot\hat{r}')}e^{-j\beta\left[\frac{r'^2}{2r}(1-(\hat{r}\cdot\hat{r}')^2)\right]}\left(\hat{z} \times \underline{E}(\underline{r}')\right)dx'dy', \tag{39}$$

$$\underline{H}_F = \frac{1}{\zeta}\hat{r} \times \underline{E}_F. \tag{40}$$

The discussion and the properties are the same as in Section 2.2.

It should be noticed that a slightly different version of (36) was derived in [44] by exploiting scalar diffraction theory, which rephrases (36) as

$$\frac{2D^2}{\lambda} > r > 0.5D\sqrt{\frac{D}{\lambda}}. \tag{41}$$

3.3. The Paraxial Approximation for the Fraunhofer Region

The paraxial Fraunhofer region is that portion of space wherein the fields can be calculated following the assumptions [4,6]

$$z \gg D + L; \tag{42a}$$

$$z \gg \lambda; \tag{42b}$$

$$z > \frac{1}{2}(L + D)\sqrt[3]{\frac{L + D}{\lambda}};\ z > 2\frac{D^2}{\lambda}. \tag{42c}$$

The first two conditions, (42a) and (42b), allow the approximation of the "amplitude terms" in Equations (31) and (32) as:

$$\frac{z}{R}\left(1 + \frac{1}{j\beta R}\right)\hat{R} \cong \hat{z}, \tag{43}$$

$$\frac{z}{R}\left[\left(\underline{\underline{I}} - \hat{R}\hat{R}\right) + \left(\underline{\underline{I}} - 3\hat{R}\hat{R}\right)\left(\frac{1}{j\beta R} + \frac{1}{(j\beta R)^2}\right)\right] \cong \left(\underline{\underline{I}} - \hat{z}\hat{z}\right) = \hat{z} \times ((\cdot) \times \hat{z}), \tag{44}$$

where $\hat{z} \times ((\cdot) \times \hat{z})$ should be understood under the meaning illustrated after Equation (12).

After setting $\underline{R} = z\hat{z} + \Delta\underline{R}_t$ where $\Delta\underline{R}_t = \underline{r}_t - \underline{r}_t{}'$, with $\underline{r}_t = x\hat{x} + y\hat{y}$ and $\underline{r}_t{}' = x'\hat{x} + y'\hat{y}$, condition (42c) enables the following approximation for the exponential term in Equations (31) and (32):

$$e^{-j\beta(R-z)} \cong e^{-j\beta\frac{(x^2+y^2)}{2z}} e^{j\beta\frac{(xx'+yy')}{z}}. \tag{45}$$

In Equation (45), terms of higher order than the second in $\frac{|\Delta\underline{R}_t|}{z}$ as well as terms of the second order in $\frac{x'}{z}$ and $\frac{y'}{z}$, are assumed to be negligible. In particular, the first neglected term in $\frac{|\Delta\underline{R}_t|}{z}$, namely, the quartic one in $\frac{|\Delta\underline{R}_t|}{z}$, is supposed as the most relevant one with respect to the reminders, such that:

$$e^{-j\beta z\frac{1}{8}\left(\frac{|\Delta\underline{R}_t|}{z}\right)^4} \cong 1. \tag{46}$$

Coherently with [4], the usual criterion to accept the approximation in Equation (46) is:

$$\frac{\beta}{8}\frac{\left[\frac{D+L}{2}\right]^4}{z^3} < \frac{\pi}{8} \leftrightarrow z > \frac{1}{2}(D+L)\sqrt[3]{\frac{D+L}{\lambda}}. \tag{47}$$

where the maximum value for $|\Delta\underline{R}_t|$ is obviously set to be equal to $\frac{D+L}{2}$ to consider the worst case. Furthermore, concerning the terms of the second order in $\frac{x'}{z}$ and $\frac{y'}{z}$, it is assumed that:

$$e^{-j\beta z\frac{1}{2}\left(\frac{x'^2+y'^2}{z^2}\right)} \cong 1. \tag{48}$$

Again, coherently with [4], when the worst case is considered, the usual criterion to accept the approximation in Equation (48) gives:

$$\frac{\beta}{2}\frac{\left[\frac{D}{2}\right]^2}{z} < \frac{\pi}{8} \leftrightarrow z > 2\frac{D^2}{\lambda}. \tag{49}$$

After Equations (43)–(45), the field expressions turn into:

$$\underline{E}_{P_\infty}(\underline{r}) = \frac{j\beta}{2\pi}\frac{e^{-j\beta z}}{z} e^{-j\beta\frac{(x^2+y^2)}{2z}} \iint_A e^{j\beta\frac{(xx'+yy')}{z}} \underline{E}_a(\underline{r}')dx'dy\prime, \tag{50}$$

$$\underline{H}_{P_\infty}(\underline{r}) = \frac{1}{\zeta}\hat{z} \times \underline{E}_{P_\infty}(\underline{r}). \tag{51}$$

where $\underline{E}_a = \hat{z} \times (\underline{E} \times \hat{z})$ is the canonical aperture E-Field. Equation (50) establishes a Fourier transform relationship between the aperture field and the far field. Accordingly, from Equations (50) and (51), the fields in the Fraunhofer region can be calculated by exploiting the Fourier integrals.

The fields in the paraxial Fraunhofer region satisfy the following properties:

- $\underline{E}_{P_\infty} \cdot \hat{z} = 0$;
- $\underline{H}_{P_\infty} \cdot \hat{z} = 0$;
- $\underline{E}_{P_\infty} = \zeta \underline{H}_{P_\infty} \times \hat{z}$;
- $\underline{S}_{P_\infty} = \frac{1}{2\zeta^*}\left|\underline{E}_{P_\infty}\right|^2\hat{z} = \frac{\zeta}{2}\left|\underline{H}_{P_\infty}\right|^2\hat{z}$.

As can be seen, the properties of the fields in the paraxial Fraunhofer approximation are very similar to those in the standard case (see Section 2.1), but with $\hat{z}$ instead of $\hat{r}$.

It should be noticed that a different Fraunhofer condition, alternative to (42c), was given in [43] for a uniformly illuminated circular aperture. In particular, the Fraunhofer boundary was defined as that for which the relative amplitude error achieved by approximating the electric field in Equation (29) with that in Equation (50) along the z-axis is less than a certain, preassigned real relative error Δe. Under such an assumption, the Fraunhofer boundary (42c) becomes

$$z \geq \frac{\pi D^2}{4\lambda \sqrt[3]{24\Delta e}}. \tag{52}$$

3.4. The Paraxial Approximation for the Fresnel Region

The paraxial Fresnel region is that portion of space wherein the fields can be calculated following the assumptions [4,6]

$$z \gg D + L; \tag{53a}$$

$$z \gg \lambda; \tag{53b}$$

$$2\frac{D^2}{\lambda} > z > \frac{1}{2}(L + D)\sqrt[3]{\frac{L + D}{\lambda}}. \tag{53c}$$

Conditions (53a) and (53b) allow the same approximations expressed by Equations (43) and (44) and exploited in Equations (31) and (32) for the foregoing case of the Fraunhofer region. On the other side, under condition (53c), the approximations in Equations (45) and (46) do not hold anymore. In more detail, Equation (45) turns into:

$$e^{-j\beta(R-z)} \cong e^{-j\beta\frac{(x^2+y^2)}{2z}} e^{j\beta\frac{(x'^2+y'^2)}{2z}} e^{j\beta\frac{(xx'+yy')}{z}}. \tag{54}$$

Following Equations (43), (44), and (54), the field expressions turn into the following:

$$\underline{E}_{P_F}(\underline{r}) = \frac{j\beta}{2\pi}\frac{e^{-j\beta z}}{z} e^{-j\beta\frac{(x^2+y^2)}{2z}} \iint_A e^{j\beta\frac{(x'^2+y'^2)}{2z}} e^{j\beta\frac{(xx'+yy')}{z}} \underline{E}_a(\underline{r}')dx'dy', \tag{55}$$

$$\underline{H}_{P_F}(\underline{r}) = \frac{1}{\zeta}\hat{z} \times \underline{E}_{P_F}(\underline{r}). \tag{56}$$

As can be seen from Equation (55), the fields in the paraxial Fresnel region can be calculated by exploiting the Fresnel integrals [6], and they satisfy the following conditions, as stated by Equations (55) and (56):

- $\underline{E}_{P_F} \cdot \hat{z} = 0$;
- $\underline{H}_{P_F} \cdot \hat{z} = 0$;
- $\underline{E}_{P_F} = \zeta \underline{H}_{P_F} \times \hat{z}$;
- $\underline{S}_{P_F} = \frac{1}{2\zeta}\left|\underline{E}_{P_F}\right|^2 \hat{z} = \frac{\zeta}{2}\left|\underline{H}_{P_F}\right|^2 \hat{z}$.

As can be seen, the properties of the fields in the paraxial Fresnel approximation are very similar to those in the standard case (see Section 2.2), but with $\hat{z}$ instead of $\hat{r}$.

We finally notice that the validity of the paraxial Fresnel approximation has been widely discussed throughout the literature, especially in the 1980s. A slightly different version of Equation (53c) was derived for the first time in [45] by using the Kirchhoff scalar theory and assuming a maximum phase error of $\frac{\pi}{2}$ instead of $\frac{\pi}{8}$ to be acceptable. Under such an assumption, Equation (53c) becomes

$$2\frac{D^2}{\lambda} > z > (L + D)\sqrt[3]{\frac{L + D}{2\lambda}}. \tag{57}$$

It should be also mentioned that an estimate of the angular sector under which the paraxial Fresnel approximation holds true was derived in [46]. In particular, it was found that the angular sector width is approximately 18° in practical cases.

Notably, some authors distinguish, within the paraxial Fresnel region, the so-called Rayleigh region, which settles down to distances less than $\frac{D^2}{2\lambda}$ [47]. In this region, radiation is concentrated within a tubular beam and the radiated wave is quasi-planar.

3.5. Applications of the Paraxial Approximations

Paraxial approximations are of interest in array beamforming [48] (Fresnel Region), in radar cross section (RCS) calculations [49] (far-field region) [50] (Fresnel region), and in Gaussian beam radiation and complex source characterizations [51] (far-field region). In optics, it is of interest for short-pulse emissions [52] (far-field region), for optical beam characterization [53] (far-field region), in holography [54] (Fresnel region), and in lens design [55] (Fresnel region).

4. Sources Small with Respect to the Wavelength λ

In this section, we point out how the case of a source whose dimensions are small with respect to the wavelength λ is discussed throughout the literature with a slightly different perspective than what has been considered previously [7].

At variance with electrically large radiators which may involve several parameters to radiate complex (e.g., shaped) beams [56], electrically small antennas generate simpler patterns, and the main parameters that challenge their synthesis are the bandwidth (Q factor) and radiating efficiency [57–60]. Concerning placement, although the complex patterns of electrically large antennas can interact with the environment in a specific way, and specific synthesis tools accommodating near-field constraints are required [61], the supporting structure of electrically small antennas can typically contribute to the radiation [62], and this should be properly accounted for during the placement.

As in Section 2, the smallest sphere B containing the source is considered. It has diameter D, and the $Oxyz$ reference system is assumed to be centered at the center of B (see Figure 3).

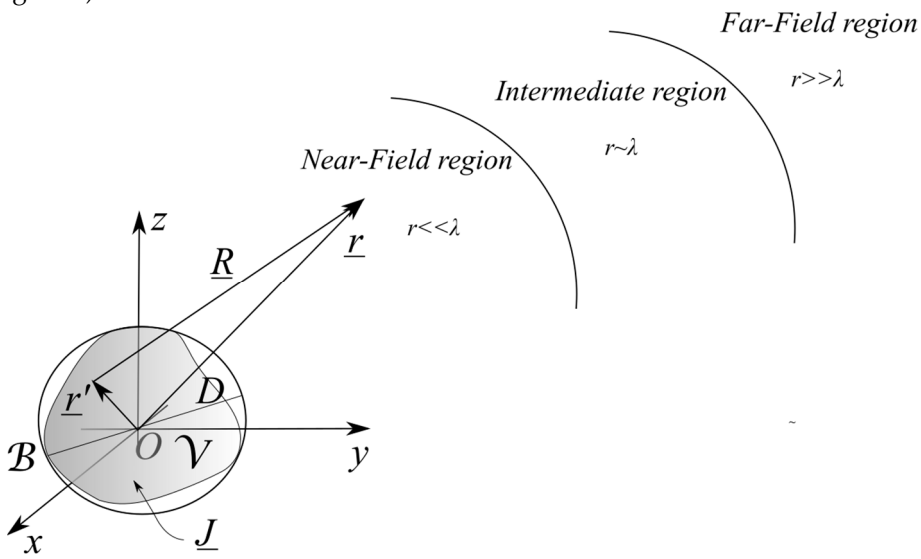

Figure 3. Small sources with respect to the wavelength λ.

A small source has $D \ll \lambda$. The region of interest is that outside the source, i.e., that for $r > \frac{D}{2}$.

In the discussion below, the electric dipole moment $\underline{p}$ of the source is introduced and defined as:

$$\underline{p}(\underline{r}) = \iiint_{\mathcal{B}} \underline{r}'\rho(\underline{r}')d\mathrm{V}, \tag{58}$$

where ρ is the electric charge density, related to the current density $\underline{J}$ by the continuity equation: $\nabla \underline{J} + j\omega\rho = 0$.

4.1. The Fraunhofer or Far-Field Region

The Fraunhofer region can be defined exactly as it is in Section 2. Obviously, the three conditions (9a)–(9c) reduce to just one:

$$r \gg \lambda. \tag{59}$$

Following (59), the potential $\underline{A}$ in Equation (1) can be re-written as:

$$\underline{A}_{\infty}(\underline{r}) = \frac{\mu}{4\pi}\frac{e^{-j\beta r}}{r}\iiint_{\mathcal{B}} \underline{J}(\underline{r}')e^{j\beta r'(\hat{r}\cdot\hat{r}')}\mathrm{dV}. \tag{60}$$

In Equation (60), the exponential term can be expanded in a power series, leading to the expression:

$$\underline{A}_{\infty}(\underline{r}) = \frac{\mu}{4\pi}\frac{e^{-j\beta r}}{r}\sum_{n=0}^{+\infty}\frac{(j\beta)^n}{n!}\iiint_{\mathcal{B}} \underline{J}(\underline{r}')\left(r'\left(\hat{r}\cdot\hat{r}'\right)\right)^n\mathrm{dV}. \tag{61}$$

For small sources, only few terms of the summation in Equation (61) can be retained. In particular, when just the first term is considered, $\underline{A}_{\infty}$ can be expressed as:

$$\underline{A}_{\infty}(\underline{r}) \cong \frac{\mu}{4\pi}\frac{e^{-j\beta r}}{r}\iiint_{\mathcal{B}} \underline{J}(\underline{r}')\mathrm{dV}. \tag{62}$$

From Equations (58) and (62), the following expression for the potential $\underline{A}_{\infty}$ follows immediately using integration by parts [7]:

$$\underline{A}_{\infty}(\underline{r}) \cong \frac{\mu}{4\pi}\frac{e^{-j\beta r}}{r}j\omega\underline{p}. \tag{63}$$

It should be noticed that the vector potential in Equation (63) determines the field of an electric elementary dipole with a moment in Equation (58). When further terms in Equation (61) are considered, the magnetic dipole or the quadrupole electric terms appear.

The field $\underline{E}$ and $\underline{H}$ in the Fraunhofer region associated with Equation (63) can be obtained immediately from $\underline{A}_{\infty}$, thanks to standard relationships. In particular [7],

$$\underline{E}(\underline{r}) = \frac{\beta^2}{4\pi\varepsilon_0}\left\{\hat{r}\times\left(\underline{p}\times\hat{r}\right)\left(1+\frac{1}{j\beta r}+\frac{1}{(j\beta r)^2}\right)-2\hat{r}\left(\underline{p}\cdot\hat{r}\right)\left(\frac{1}{j\beta r}+\frac{1}{(j\beta r)^2}\right)\right\}\frac{e^{-j\beta r}}{r}, \tag{64}$$

$$\underline{H}(\underline{r}) = \frac{c\beta^2}{4\pi}\left(\hat{r}\times\underline{p}\right)\left(1+\frac{1}{j\beta r}\right)\frac{e^{-j\beta r}}{r}. \tag{65}$$

The question of when condition (59) should be considered to be met from a practical point of view, namely, of how much larger r should be than λ to be in the Fraunhofer region, has been discussed often throughout the literature and depends on the applicative framework of interest.

In applications of electromagnetic compatibility (EMC) or electromagnetic field measurements (EFMs) for compatibility applications [63,64], the far-field boundary is often determined at the distance at which the terms in $\frac{1}{\beta r}$ in (64) and (65), namely, $\frac{1}{\beta r}$, $\frac{1}{(\beta r)^2}$, and $\frac{1}{(\beta r)^3}$, have the same magnitude. This requires that $\beta r = 1$, or

$$r = \frac{\lambda}{2\pi}, \tag{66}$$

The boundary (66) is typically used for electrically small antennas in applications of low-frequency EMC/EMF.

In applications of EMC/EMF [63,64], the field should have a character of a local plane-wave. Accordingly, the far-field boundary is located at a distance corresponding to the region for which the ratio between the amplitudes of the components of $\underline{E}$ and $\underline{H}$ transverse to $\hat{r}$ is approximately equal to ζ. Referring to Equations (64) and (65), we notice that $\underline{H}$ is fully transverse to $\hat{r}$, while the transverse component of $\underline{E}$ is:

$$\underline{E}_t(\underline{r}) = \frac{\beta^2}{4\pi\varepsilon_0}\left\{\hat{r}\times\left(\underline{p}\times\hat{r}\right)\left(1+\frac{1}{j\beta r}+\frac{1}{(j\beta r)^2}\right)\right\}\frac{e^{-j\beta r}}{r}, \tag{67}$$

Accordingly, the ratio at hand is provided by [63]:

$$\zeta\frac{\left(1+\frac{1}{j\beta r}+\frac{1}{(j\beta r)^2}\right)}{\left(1+\frac{1}{j\beta r}\right)}, \tag{68}$$

It can be verified that (68) can be approximated to ζ when

$$r > \frac{5\lambda}{2\pi}. \tag{69}$$

When the source has size $D < \frac{\lambda}{3}$, it was numerically found in [28] that the operating condition is:

$$r > 1.6\lambda. \tag{70}$$

In [27], it was shown that condition (70) leads to a relative error between the wave impedance (68) and ζ less than 1%, as well as a ratio between active and reactive power less than -30 dB.

More restrictive conditions were derived in [27]. In particular, by requesting that the far-field of an infinitesimal dipole be approximately a spherical wave, namely, that the reactive terms $\frac{1}{(\beta r)^2}$ and $\frac{1}{(\beta r)^3}$ be negligible with respect to the radiative term $\frac{1}{\beta r}$, the following condition was determined:

$$r > 5\lambda. \tag{71}$$

Again, in [27], by requesting that the radial field components be negligible as compared to the transverse ones, the following condition was reached instead:

$$r > 10\lambda. \tag{72}$$

The far-field conditions were also analyzed in [26,65] with reference to antennas radiating above a ground. In particular, in [65], the case of a perfectly electric conducting (PEC) soil was dealt with, and the radiation of elementary dipoles located either vertically or horizontally at a certain quota h_{TX} was investigated (see Figure 4).

For the case of a vertically located dipole, two criteria were considered to define the Fraunhofer region. With the former, the far-field region is defined as the region starting from which the field decays as $\frac{1}{r}$, while, with the second criterion, the Fraunhofer boundary is set at a distance from the source at which the ratio of the radial and transverse field components becomes less than a threshold fixed at -40 dB. The first criterion leads to

$$D = \frac{2\pi h_{TX}h_{RX}}{\lambda} \tag{73}$$

and the second to:

$$D = 10H_{TX}\sqrt{\frac{2\pi h_{RX}}{\lambda}}. \tag{74}$$

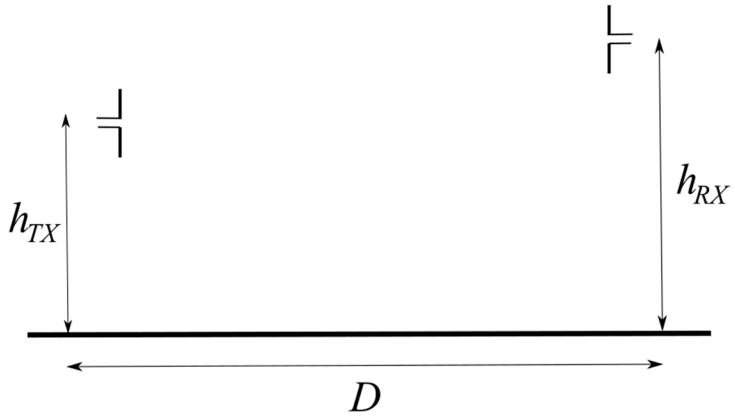

Figure 4. Small antennas in presence of a ground.

In [26], it was verified that condition (74) is also sufficient to define the Fraunhofer boundary in the case of a ground with finite conductivity.

4.2. The Near-Field Region

The near-field region is that region defined by the condition:

$$r \ll \lambda. \tag{75}$$

Thanks to (75), the exponential term in Equation (1) can be approximated as:

$$e^{-j\beta R} \cong 1, \tag{76}$$

so that, in this region:

$$\underline{A}(\underline{r}) \cong \frac{\mu}{4\pi} \iiint_{\mathcal{B}} \frac{\underline{J}(\underline{r}')}{R} \mathrm{dV}. \tag{77}$$

It should be remarked that the quantity $\frac{1}{R}$ in Equation (77) can be expanded in scalar spherical harmonics as in the static case [7]. The fields that can be calculated from Equation (77) are quasi-stationary in the sense that they oscillate in time as $e^{j\omega t}$, but in terms of other characteristics, they are very similar to the static case [7].

It should be finally noticed that, in [66–68], indications of the possibility of defining the near-field region boundary for elementary sources were given. In particular, in [66–68], an elementary electric dipole was considered, and the phase shift $\Delta\varphi$ between the transverse components of electric and magnetic fields was examined against the distance r from the source, obtaining

$$r = \frac{\lambda}{2\pi} \sqrt[3]{cotg\Delta\varphi}. \tag{78}$$

Taking into account that, in the near-field region of an elementary dipole, $\Delta\varphi \cong \frac{\pi}{2}$, then Equation (78) can be exploited to define the near-field boundary of small antennas as the boundary where a maximum tolerable deviation of $\Delta\varphi$ from $\frac{\pi}{2}$ is reached.

4.3. The Intermediate Region

The intermediate region is defined by the condition:

$$\lambda \sim r. \tag{79}$$

In the intermediate region, the approximations introduced for the two other regions cannot be applied, and the expression of the fields remain general.

In some cases, the intermediate region is defined starting from the ratio between the amplitudes of the electric and magnetic fields. In [63], after evaluating such a ratio numerically for an elementary source, the intermediate region was defined by:

$$0.1\frac{\lambda}{2\pi} < r < 0.8\frac{\lambda}{2\pi}, \tag{80}$$

as the region where the above ratio achieves a minimum before blowing up for $r < 0.1\frac{\lambda}{2\pi}$.

5. The Reactive and the Radiative Regions

The space around an antenna can be partitioned following a criterion alternative to those introduced in the previous sections. Two regions can be identified, according to the contribution to the reactive field components: the reactive region and the radiative region.

In particular, in close proximity to the antenna, the field strength may include, in addition to the radiating field, a significant reactive (non-radiating) field. However, the strength of the reactive-field components decays rapidly with the distance from the antenna, and that region of space immediately surrounding the antenna in which the reactive components predominate is known as the reactive (near-field) region.

To clarify this point, the case of a planar aperture is, hence, considered and analyzed with the aid of the plane wave spectrum (PWS) representation. In practice, the analysis is of interest for sources fully embedded in a half-space and "in close proximity" to the aperture plane, as shown in Figure 5.

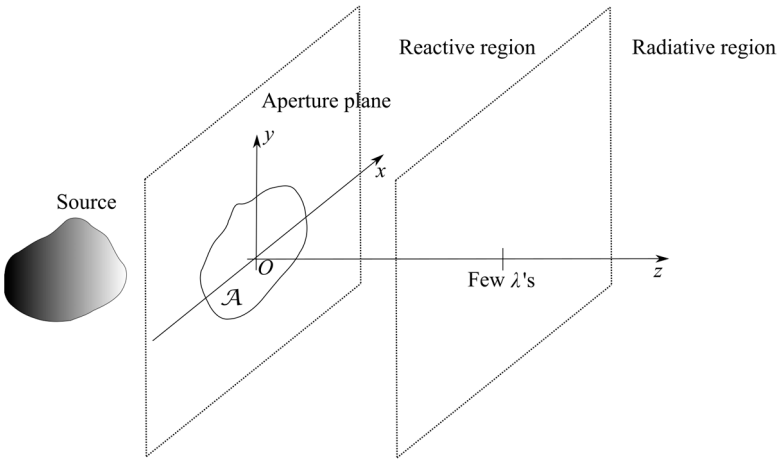

Figure 5. The reactive and the radiative regions.

It should be mentioned that, to deal with an exemplary case, we are considering a planar geometry. Nevertheless, an analogous analysis for other geometries, such as cylindrical or spherical ones, can be made possible by resorting to tailored field representations.

Given a $Oxyz$ reference system, the $z = 0$ plane is assumed to be the aperture plane, while the $z > 0$ half-space is assumed to be source-free, as usual, and the medium therein homogeneous and lossless, as above. The source is supposed to be accommodated in the $z < 0$ half-space.

The size of the reactive/radiative regions depends on the considered source. For most antennas, however, the outer limit of the reactive region is of the order of a few wavelengths or less.

In the example worked out below, the conditions can be written as:

$$\text{Reactive region}: \ z \leq \text{few } \lambda, \tag{81}$$

$$\text{Radiative region}: \ z \geq \text{few } \lambda, \tag{82}$$

Indeed, according to the PWS representation [5], the electric field can be written, in the z > 0 half-space, as:

$$\underline{E}(\underline{r}) = \frac{1}{2\pi}\iint_{-\infty}^{+\infty} \underline{T}(k_x, k_y) e^{-j(k_x x + k_y y + k_z z)} dk_x dk_y, \tag{83}$$

where

$$k_z = \begin{cases} \beta_z = \left|\sqrt{\beta^2 - k_x^2 - k_y^2}\right|, \ k_x^2 + k_y^2 \leq \beta^2, \text{ i.e., } (k_x, k_y) \in C_V \\ -j\alpha_z = -j\left|\sqrt{k_x^2 + k_y^2 - \beta^2}\right|, \ k_x^2 + k_y^2 > \beta^2, \text{ i.e., } (k_x, k_y) \in C_I \end{cases}, \tag{84}$$

C_V and C_I are the so-called visible and invisible regions, respectively,

$$\underline{T}(k_x, k_y) = \frac{e^{jk_z z}}{2\pi}\iint_{-\infty}^{+\infty} \underline{E}(x, y, z) e^{j(k_x x + k_y y)} dx dy, \tag{85}$$

$\underline{T}$ is the plane wave spectrum of $\underline{E}$.

By denoting with P and Q the active and reactive power flowing through a plane orthogonal to the z axis, with abscissa $z > 0$, respectively, Equations (83) and (85) immediately give [5]:

$$\left|\frac{Q}{P}\right| = \left|\frac{\iint_{C_I} \alpha_z \left(2|\hat{z}\cdot\underline{T}|^2 - |\underline{T}|^2\right) e^{-2\alpha_z z} dk_x dk_y}{\iint_{C_V} \beta_z |\underline{T}|^2 dk_x dk_y}\right|. \tag{86}$$

After straightforward manipulations of Equation (86), a (non-narrow) bound to $\left|\frac{Q}{P}\right|$ can be obtained as:

$$\left|\frac{Q}{P}\right| \leq \left|\frac{\int_0^{2\pi} d\eta \int_0^{+\infty} d\xi \cosh(\xi) |\underline{F}_I(\xi, \eta)|^2 e^{-2\beta_z \sinh(\xi)}}{\int_0^{2\pi} d\varphi \int_0^{\frac{\pi}{2}} d\vartheta \sin(\vartheta) |\underline{F}_V(\vartheta, \varphi)|^2}\right|, \tag{87}$$

where $\underline{F}$ is the far-field function, defined as:

$$\begin{cases} \underline{F}_V(\vartheta, \varphi) = \beta\cos(\vartheta)\underline{T}(\beta\sin(\vartheta)\cos(\varphi), \beta\sin(\vartheta)\sin(\varphi)), \ \vartheta\epsilon\left(0, \frac{\pi}{2}\right), \varphi\epsilon(0, 2\pi) \\ \underline{F}_I(\xi, \eta) = \beta\sinh(\xi)\underline{T}(\beta\cosh(\xi)\cos(\eta), \beta\cosh(\xi)\sin(\eta)), \ \xi\epsilon(0, +\infty), \eta\epsilon\ (0, 2\pi) \end{cases}. \tag{88}$$

The use of the far-field function in place of $\underline{T}$ is convenient, since it is free from singularities.

With the domains of integration connected and the integrands regular, the integral mean-value theorem can be applied [69]. The inequality (87) then becomes:

$$\left|\frac{Q}{P}\right| \leq \frac{\left(|\underline{F}|^2\right)_I}{\left(|\underline{F}|^2\right)_V} \frac{1}{2\beta_z}, \tag{89}$$

where $\left(|\underline{F}|^2\right)_V$ and $\left(|\underline{F}|^2\right)_I$ represent the weighted means of $|\underline{F}|^2$ in the visible and invisible portions of the spectrum, respectively.

As long as $\left(|\underline{F}|^2\right)_I$ has an order no larger than $\left(|\underline{F}|^2\right)_V$, a hypothesis frequently verified in practice following Equation (89) for an increasing z, the ratio $\left|\frac{Q}{P}\right|$ becomes smaller than $\frac{1}{10}$ when $z \sim \lambda$. Accordingly, conditions (81) and (82) follow.

Conditions (81) and (82) are universally accepted throughout the literature. Nevertheless, non-standard proposals have been also presented. In particular, the ratio $\left|\frac{Q}{P}\right|$ was numerically analyzed in [70] by referring to circular apertures with different kinds of illuminations and with reference to uniformly illuminated rectangular apertures. It

has been observed that such a ratio remains larger than -30 dB within a region whose size is approximately $\frac{D^2}{8\lambda}$, namely, one-fourth of the Rayleigh distance. Again, in [64], it was observed how the same boundary applies to the condition that the wave impedance, evaluated as the ratio between electric and magnetic field amplitudes, differs from the free space one of more than 1%. The authors of [70] thus suggested, as a starting distance for the near-field region, a distance equal to $\frac{D^2}{8\lambda}$.

In the reactive region, the reactive field components are responsible for the continuously changing interference between the contributions of each individual point of the aperture to the field over the observation plane, as long as the reciprocal distance between the observation and aperture planes changes.

6. Summary

In this paper [71], the field regions and their boundaries around a source are reviewed. The attention is focused on the case of sources whose dimensions are comparable to or larger than the wavelength, of planar sources/apertures, of sources whose dimensions are small with respect to the wavelength, and on the criteria involving the strength of the reactive components of the field with respect to those of the radiative ones.

The Fraunhofer and the Fresnel regions are detailed, with reference to the paraxial case for planar apertures. The near-field and intermediate regions are also discussed.

The standard, universally accepted region conditions are considered. Nevertheless, many threads of work carried out by different authors who have proposed alternative conditions over the years, depending on the applicative framework and based typically on numerical arguments, are considered as points of discussion.

In summary, we present not only a literature review of electromagnetic field zones, but also the related analytical derivations. Indeed, as the field zones' boundaries are conventional, being aware of their analytical rationales would help us to understand whether they could be useful for the applications of interest.

Author Contributions: All the authors have equally contributed to the paper. All authors have read and agreed to the published version of the manuscript.

Funding: This research received no external funding.

Conflicts of Interest: The authors declare no conflicts of interest.

Appendix A

In this Appendix, we shortly resume Ref. [72], in which the antenna reception process is formulated through a linear functional underlying the importance of approximating the field impinging on the receiving antenna as a plane wave.

We assume that the receiving antenna is an aperture antenna with aperture $\mathcal{A}_R$ and that it is made of linear materials and linear components. Under such assumptions, the relationship between the field impinging over $\mathcal{A}_R$ and the open circuit voltage V is represented by the following linear function:

$$\mathcal{M}|\underline{E}_i \rightarrow \mathcal{M}(\underline{E}_i) = \langle \underline{E}_i, \underline{M} \rangle = V, \tag{A1}$$

where $\underline{E}_i$ contains the relevant vector components of the field incident all over $\mathcal{A}_R$, $\mathcal{M}$ returns the signal from the impinging field, $\langle \cdot, \cdot \rangle$ stands for the duality, and $\underline{M}$ is the vector function representing the functional $\mathcal{M}$ in the dual space of the fields.

Accordingly, using the Ritz Theorem [73], and for a planar aperture, $\mathcal{M}$ can be expressed as a scalar product:

$$\mathcal{M}|\underline{E}_i \rightarrow \iint_{\mathcal{A}_R} \underline{E}_i(x,y) \cdot \underline{m}^*(x,y) dxdy = V, \tag{A2}$$

where $\underline{m}(x,y)$ represents the sensing function and generalizes the concept of effective length.

In the case where $\underline{E}_i$ can be approximated by a plane wave over $\mathcal{A}_R$, namely, $\underline{E}_i = \underline{E}_{i_0} \exp\left(-j\beta\hat{k}\cdot\underline{r}\right)$, where $\underline{r}$ is the position vector and $\hat{k}$ is the unit propagation vector, upon substituting the plane wave expression in (A2), V turns into

$$V = \underline{E}_{i_0} \cdot \underline{l}_e\left(\hat{k}\right) \tag{A3}$$

which expresses the well-known concept of effective length $\underline{l}_e$ of the receiving antenna.

References

1. Silver, S. *Microwave Antenna Theory and Design*; McGraw-Hill: New York, NY, USA, 1949.
2. Collin, R.E.; Zucker, F.J. *Antenna Theory, Part I*; McGraw-Hill: New York, NY, USA, 1969.
3. Born, M.; Wolf, E. *Principles of Optics*; Pergamon Press: London, UK, 2013.
4. Goodman, J. *Introduction to Fourier Optics*; McGraw-Hill: New York, NY, USA, 1996.
5. Hansen, T.; Yaghjian, A. *Plane-Wave Theory in the Time Domain*; IEEE Press: New York, NY, USA, 1999.
6. Walter, C. *Traveling Wave Antennas*; Dover Publications: New York, NY, USA, 1970.
7. Jackson, J. *Classical Electrodynamics*; Wiley: New York, NY, USA, 1999.
8. Rappaport, T. *Wireless Communications: Principles and Practice*; Horizon House Publications, Inc.: Norwood, MA, USA, 2002.
9. Barrar, R.; Wilcox, C. On the Fresnel approximation. *IRE Trans. Antennas Prop.* **1958**, *6*, 43–48. [CrossRef]
10. Baumgartner, P.; Bauernfeind, T.; Renhart, W.; Bíró, O. Numerical investigations of the field regions for wide-band antenna systems. *IEEE Trans. Magn.* **2020**, *56*, 1–4. [CrossRef]
11. Pace, J. Asymptotic formulas for coupling between two antennas in the Fresnel region. *IEEE Trans. Antennas Prop.* **1969**, *17*, 285–291. [CrossRef]
12. Southwell, W. Validity of the Fresnel approximation in the near field. *J. Opt. Soc. A.* **1981**, *71*, 7–14. [CrossRef]
13. Polk, C. Optical Fresnel-zone gain of a rectangular aperture. *IRE Trans. Antennas Prop.* **1956**, *4*, 65–69. [CrossRef]
14. Oh, S.; Yun, J.-H. New method for predicting the electromagnetic field at a finite distance using Fresnel field transformation. *IEEE Antennas Wireless Prop. Lett.* **2008**, *7*, 291–293.
15. Kim, I.; Xu, S.; Rahmat-Samii, Y. Generalised correction to the Friis formula: Quick determination of the coupling in the Fresnel region. *IET Microw. Antennas Prop.* **2013**, *7*, 1092–1101. [CrossRef]
16. Liu, L.; Matolak, D.; Tao, C.; Lu, Y.; Chen, H. Far region boundary definition of linear massive MIMO antenna arrays. In Proceedings of the IEEE 82nd Vehicular Technology Conference (VTC2015-Fall), Boston, MA, USA, 6–9 September 2015.
17. Kay, A. Near-field gain of aperture antennas. *IRE Trans. Antennas Prop.* **1960**, *8*, 586–593. [CrossRef]
18. Balanis, C. *Advanced Engineering Electromagnetics*; Wiley & Sons: Danverse, MA, USA, 2012.
19. Balanis, C. *Antenna Theory, Analysis and Design*, 3rd ed.; Wiley & Sons: Hoboken, NJ, USA, 2005.
20. IEEE recommended practice for antenna measurements. *IEEE Std.* **2022**, *149–2021*, 1–207.
21. de Bruijn, N. *Asymptotic Methods in Analysis*; North-Holland: Amsterdam, The Netherlands, 1958.
22. Hacker, P.; Schrank, H. Range distance requirements for measuring low and ultralow sidelobe antenna patterns. *IEEE Trans. Antennas Prop.* **1982**, *30*, 956–966. [CrossRef]
23. Vallauri, R.; Bertin, G.; Gianola, P.; Piovano, B. Electromagnetic field zones around an antenna for human exposure assessment: Evaluation of the human exposure to EMFs. *IEEE Antennas Prop. Mag.* **2015**, *57*, 53–63. [CrossRef]
24. Hollis, J.; Lyon, T.; Clayton, L. *Microwave Antenna Measurements*; Scientific Atlanta Inc.: Atlanta, GA, USA, 1969.
25. Tsaliovich, A.; Haridim, M.; Gavan, J. A critical note on the engineering model of radiating antenna in homogeneous medium: Field regions and transition zone boundaries. *IEEE Electromagn. Compat. Mag.* **2021**, *10*, 41–50. [CrossRef]
26. Abdallah, M.; Sarkar, T.; Salazar-Palma, M.; Monebhurrun, V. Where does the far-field of an antenna start? *IEEE Antennas Prop. Mag.* **2016**, *58*, 115–124. [CrossRef]
27. Laybros, S.; Combes, P. On radiating-zone boundaries of short, lambda/2, and lambda dipoles. *IEEE Antennas Prop. Mag.* **2004**, *46*, 63–64.
28. Bansal, R. The far-field: How far is far enough? *Appl. Microw. Wirel.* **1999**, *11*, 58–60.
29. Buchanan, M.D.; Moore, R.K. *Fresnel Zone Processing of Synthetic Aperture Radar Data*; Remote Sensing Laboratory, Technical Report 61-1; The University of Kansas: Lawrence, Kansas, 1966.
30. Sierra-Castañer, M.; Burgos, S. Fresnel zone to far field algorithm for rapid array antenna measurements. In Proceedings of the 5th European Conference on Antennas and Propagation (EUCAP), Rome, Italy, 11–15 April 2011; pp. 3251–3255.
31. Grella, R. Fresnel propagation and diffraction and paraxial wave equation. *J. Opt.* **1982**, *13*, 367–374. [CrossRef]
32. Pierri, R.; Soldovieri, F. On the information content of the radiated fields in the near zone over bounded domains. *Inv. Probl.* **1998**, *14*, 321–337. [CrossRef]
33. Agayan, G.M. Numerical solution of the problem of image formation in two planes using the integral Fresnel formula. *Comput. Math. Model.* **2000**, *11*, 75–78. [CrossRef]
34. Junchang, L.; Yanmei, W. An indirect algorithm of Fresnel diffraction. *Opt. Commun.* **2009**, *282*, 455–458. [CrossRef]
35. Lecklider, T. The world of the near field. *Eval. Eng.* **2005**, *44*, 52–57.

36. Pawlak, R.; Krawiec, P.; Żurek, J. On measuring electromagnetic fields in 5G technology. *IEEE Access* **2019**, *7*, 29826–29835. [CrossRef]
37. Zhang, H.; Shlezinger, N.; Guidi, F.; Dardari, D.; Eldar, Y.C. 6G wireless communications: From far-field beam steering to near-field beam focusing. *IEEE Commun. Mag.* **2023**, *61*, 72–77. [CrossRef]
38. Herrojo, C.; Moras, M.; Paredes, F.; Núñez, A.; Mata-Contreras, J.; Ramon, E.; Martín, F. Time-domain-signature chipless RFID tags: Near-field chipless-RFID systems with high data capacity. *IEEE Microw. Mag.* **2019**, *20*, 87–101. [CrossRef]
39. Coskun, V.; Ozdenizci, B.; Ok, K. The survey on Near Field Communication. *Sensors* **2015**, *15*, 13348–13405. [CrossRef] [PubMed]
40. Shao, W.; McCollough, T. Advances in Microwave Near-Field Imaging: Prototypes, Systems, and Applications. *IEEE Microw. Mag.* **2020**, *21*, 94–119. [CrossRef] [PubMed]
41. Capozzoli, A.; Curcio, C.; D'Elia, G.; Liseno, A. Singular value optimization in plane-polar near-field antenna characterization. *IEEE Antennas Prop. Mag.* **2010**, *52*, 103–112.
42. Capozzoli, A.; Curcio, C.; D'Elia, G.; Liseno, A. Phaseless antenna characterization by effective aperture field and data representations. *IEEE Trans. Antennas Prop.* **2009**, *57*, 215–230. [CrossRef]
43. Mezouari, S.; Harvey, R. Validity of Fresnel and Fraunhofer approximations in scalar diffraction. *J. Opt. A Pure Appl. Opt.* **2003**, *5*, S86–S91. [CrossRef]
44. Selvan, K.; Janaswamy, R. Fraunhofer and Fresnel distances: Unified derivation for aperture antennas. *IEEE Antennas Prop. Mag.* **2017**, *59*, 12–15. [CrossRef]
45. Rees, W. The validity of the Fresnel approximation. *Europ. J. Phys.* **1987**, *8*, 44–48. [CrossRef]
46. Ziomek, L. Three necessary conditions for the validity of the Fresnel phase approximation for the near-field beam pattern of an aperture. *IEEE J. Ocean Eng.* **1993**, *18*, 73–75. [CrossRef]
47. Combes, P.F. An experimental and theoretical study of the tubular beam from a radiating aperture. In Proceedings of the 1973 3rd European Microwave Conference, Brussels, Belgium, 4–7 September 1973; pp. 1–4.
48. Di Renzo, M.; Dardari, D.; Decarli, N. LoS MIMO-Arrays vs. LoS MIMO-Surfaces. In Proceedings of the 2023 17th European Conference on Antennas and Propagation (EuCAP), Firenze, Italy, 26–31 March 2023; pp. 1–5.
49. Zaporozhets, A.A.; Levy, M.F. Bistatic RCS calculations with the vector parabolic equation method. *IEEE Trans. Antennas Prop.* **1999**, *47*, 1688–1696. [CrossRef]
50. Nishioka, Y.; Inasawa, Y.; Tanaka, T.; Miyashita, H. Performance evaluation of RCS near-field-to-far-field transformation technique for aircrafts. In Proceedings of the 2016 International Symposium on Antennas and Propagation (ISAP), Okinawa, Japan, 24–28 October 2016; pp. 166–167.
51. Chou, H.-T.; Pathak, P.H.; Tuan, S.-C.; Burkholder, R.J. A novel far-field transformation via complex source beams for antenna near-field measurements on arbitrary surfaces. *IEEE Trans. Antennas Prop.* **2017**, *65*, 7266–7279. [CrossRef]
52. Zapata-Rodrìguez, C.J. Paraxial waves in the far-field region. *Optik* **2002**, *113*, 361–365. [CrossRef]
53. Agrawal, G.P. Far-field diffraction of pulsed optical beams in dispersive media. *Opt. Commun.* **1999**, *167*, 15–22. [CrossRef]
54. Bouchal, P.; Kapitán, J.; Chmelík, R.; Bouchal, Z. Point spread function and two-point resolution in Fresnel incoherent correlation holography. *Opt. Express* **2011**, *19*, 15603–15620. [CrossRef] [PubMed]
55. Cao, G.; Gan, X.; Lin, H.; Jia, B. An accurate design of graphene oxide ultrathin flat lens based on Rayleigh-Sommerfeld theory. *Opt. Electron. Adv.* **2018**, *1*, 180012. [CrossRef]
56. Capozzoli, A.; D'Elia, G. Global optimization and antennas synthesis and diagnosis, Part one: Concepts, tools, strategies and performances. *Progr. Electromagn. Res.* **2006**, *56*, 195–232. [CrossRef]
57. Sharma, S.K.; Nagarkoti, D.S. Meet the Challenge of Designing Electrically Small Antennas. Microwave & RF Magazine. 2017; pp. 1–4. Available online: https://www.mwrf.com/technologies/components/article/21848593/meet-the-challenge-of-designing-electricallysmall-antennas (accessed on 3 June 2024).
58. MCapek; Gustafsson, M.; Schab, K. Minimization of antenna quality factor. *IEEE Trans. Antennas Prop.* **2017**, *65*, 4115–4123.
59. Kim, O.S. Minimum Q electrically small antennas. *IEEE Trans. Antennas Prop.* **2012**, *60*, 3551–3558. [CrossRef]
60. Gustafsson, M.; Capek, M.; Schab, K. Tradeoff between antenna efficiency and Q-factor. *IEEE Trans. Antennas Prop.* **2019**, *67*, 2482–2493. [CrossRef]
61. Bucci, O.M.; Capozzoli, A.; D'Elia, G. Power pattern synthesis of reconfigurable conformal arrays with near-field constraints. *IEEE Trans. Antennas Prop.* **2004**, *52*, 132–141. [CrossRef]
62. Talashila, R.; Ramachandran, H. Determination of far fields of wire antennas on a PEC sphere using spherical harmonic expansion. *IEEE Antennas Wireless Prop. Lett.* **2019**, *18*, 646–650. [CrossRef]
63. Capps, C. *Near Field or Far Field?* Electronic Design News: Hillsboro, OR, USA, 2001; pp. 95–102.
64. Ott, H. *Noise Reduction Techniques in Electronic Systems*; Wiley & Sons: New York, NY, USA, 1988.
65. De, A.; Sarkar, T.; Salazar-Palma, M. Characterization of the far-field environment of antennas located over a ground plane and implications for cellular communication systems. *IEEE Antennas Prop. Mag.* **2010**, *52*, 19–40. [CrossRef]
66. Schantz, H. Electromagnetic energy around Hertzian dipoles. *IEEE Antennas Prop. Mag.* **2001**, *43*, 50–62. [CrossRef]
67. Schantz, H. Near field phase behavior. In Proceedings of the 2005 IEEE Antennas and Propagation Society International Symposium, Washington, DC, USA, 3–8 July 2005.
68. Schantz, H. A real-time location system using near-field electromagnetic ranging. In Proceedings of the 2007 IEEE Antennas and Propagation Society International Symposium, Honolulu, HI, USA, 8–15 June 2007.

69. Budak, B.M.; Fomin, S.V.; Volosov, V.M. *Multiple Integrals, Field Theory and Series*; MIR Publishers: Moscow, Russia, 1973.
70. Laybros, S.; Combes, P.; Mametsa, H. The "very-near-field" region of equiphase radiating apertures. *IEEE Antennas Prop. Mag.* **2005**, *47*, 50–66. [CrossRef]
71. Stutzman, W.; Thiele, G. *Antenna Theory and Design*; Wiley: New York, NY, USA, 1998.
72. Capozzoli, A.; Curcio, C.; Liseno, A. On the optimal field sensing in near-field characterization. *Sensors* **2021**, *21*, 4460. [CrossRef]
73. Rudin, W. *Functional Analysis*, 2nd ed.; McGraw-Hill Int.: Singapore, 1991.

Disclaimer/Publisher's Note: The statements, opinions and data contained in all publications are solely those of the individual author(s) and contributor(s) and not of MDPI and/or the editor(s). MDPI and/or the editor(s) disclaim responsibility for any injury to people or property resulting from any ideas, methods, instructions or products referred to in the content.